Sensitivity of predictive controllers to parameter variation in five-phase induction motor drives

Cristina Martin, Mario Bermudez Guzman, Federico Barrero, Manuel R. Arahal, Xavier Kestelyn, Mario Javier Duran

Sensitivity of Predictive Controllers to Parameter Variation in Five-Phase Induction Motor Drives

Cristina Martín[a,*], Mario Bermúdez[a,b], Federico Barrero[a], Manuel R. Arahal[c], Xavier Kestelyn[b], Mario J. Durán[d]

[a] *Dpto. Ing. Electrónica, Universidad de Sevilla, Spain*
[b] *Univ. Lille, Centrale Lille, Arts et Metiers Paris Tech, HEI, EA 2697 - L2EP Laboratoire d'Electrotechnique et d'Electronique de Puissance F-59000 Lille, France*
[c] *Dpto. Ing. de Sistemas y Automática, Universidad de Sevilla, Spain*
[d] *Dpto. Ing. Eléctrica, Universidad de Málaga, Spain*

Abstract

Model predictive control techniques have been recently proposed as a viable control alternative for power converters and electrical drives. The good current tracking, flexible control design or reduced switching losses are some of the benefits that explain the recently increased attention on finite-control-set model predictive control. The performance of the predictive model of the drive, which is the core of the predictive control, highly depends on the parameters of the real system. In this context, most research works assume good agreement between electrical parameters of the predictive model and the real machine, on the basis of nominal values. Nevertheless, this is far from being a real assumption, where non-modeled variables (i.e. the temperature, the magnetic saturation or the deep-bar effect) produce a detuning effect between the real system and its model, which can harm the control performance. The influence of parameter variations on the predictive control has barely been investigated in recent research works, where only conventional three-phase power converter configurations and permanent magnet drives have been taken into account. However, there is a lack of knowledge when different technologies like induction machines or multiphase drives are considered. It is worth highlighting the interest of the industry in induction motors as a mature technology or in multiphase drives as a promising alternative in applications where high overall system reliability and reduction in the total power per phase are required. This paper attempts to fill this gap by examining the impact of parameters mismatch on the finite-control-set predictive control performance of a five-phase induction motor drive, one of the multiphase electromechanical conversion systems with greatest impact in the research community. An exhaustive experimental sensitivity analysis of the close loop system performance based on more than three hundred trials in a test bench is presented.

Keywords: Multiphase drives, induction machines, predictive control, finite-control-set controller, sensitivity analysis.

1. Introduction

The research interest in Model Predictive Control (MPC) has appeared in recent times highly influenced by the development of modern microprocessors, whose high computational power has favored the implementation of complex and time-consuming controllers in power converters and electrical drives (Kouro et al., 2015). In this area of application, Finite-Control-Set MPC (FCS-MPC) is the most used predictive technique and appears as a promising alternative to conventional Field Oriented Control (FOC) and its principal competitor, the Direct Torque Control (DTC), due to its simplicity and flexibility to incorporate different control objectives, as well as the exhibited excellent dynamic performance (Lim et al., 2013; Rodriguez et al., 2013; Wang et al., 2014). Its extension to multiphase drives has been satisfactorily assessed in recent research works providing fast torque response and better transient performance than conventional FOC (Lim et al., 2014) and an improvement in the torque controllability with lower torque ripple comparing to the DTC (Riveros et al., 2013), since more than two system variables can be controlled at the same time.

The FCS-MPC technique is an optimization based control method, which selects at every sampling time the optimal control action (a switching state of the power converter among a finite number of possibilities) that minimizes a predefined cost function. The main challenge of FCS-MPC in real applications is the required computational burden of the optimization process, which is particularly critical in novel technologies based on multilevel converters (Vatani et al., 2015) or multiphase drives (Arahal et al., 2009; Martín et al., 2016a). On the other hand, predictive controllers are, by definition, a model based control technique and its formulation relies on the knowledge

*Corresponding author
Email addresses: cmartin15@us.es (Cristina Martín), mario.bermudez-guzman@ensam.eu (Mario Bermúdez), fbarrero@us.es (Federico Barrero), arahal@us.es (Manuel R. Arahal), xavier.kestelyn@ensam.eu (Xavier Kestelyn), mjduran@uma.es (Mario J. Durán)

of a model of the real system. When applied to the control of electrical drives, the model depends on the electrical parameters of the electrical machine, which are usually estimated using off-line techniques, such as the ones described in Chai et al. (2013), Yepes et al. (2012) and Riveros et al. (2012). However, their values usually change during the normal operation of the drive due to thermal, saturation or deep-bar effects, among others. It is well known that parameter detuning can have an important effect on the drive performance, and in Young et al. (2014) and Martín et al. (2016b) it is shown that the operating point and the model design can highly affect the performance of the system. For this reason, it is important to evaluate the parameter sensitivity of predictive controller in order to guarantee its usefulness under different operating points and conditions.

The effect of parameters mismatch in MPC has been assessed in recent research works. Thus, parameter uncertainty in a three-phase permanent magnet synchronous machine fed by a Voltage Source Inverter (VSI) is analyzed in Morel et al. (2009), Zhang et al. (2016) and Siami et al. (2016) for different MPC control schemes. Simulation and experimental results conclude that machine inductance variations are related to current ripple, whereas resistance and flux linkage variations affect to steady state errors and dynamic responses. Resistance and inductance of the predictive model of a three-phase active front end drive are detuned in Kwak et al. (2014) when it is controlled by a finite-control-set predictive controller, and an experimental analysis of the controlled system reports that inductance variations produce high current ripples and steady state errors, being negligible the effects if resistances are disturbed. A sensitivity analysis in three-phase inverters is also shown in Young et al. (2016), where it is stated that the steady state performance of the FCS-MPC is degraded when parameters are incorrect, being the load resistance in relation with steady state errors whereas changes in the load inductance increase the current ripple. All in all, previous works present a wide analysis of the predictive control dependence on the electrical parameters of the system model for different conventional power converters and drives. There is however a lack of knowledge regarding FCS-MPC applied to multiphase drives, which represent an interesting research field (Levi et al., 2016) and promising industry technology (Jung et al., 2012; Liu et al., 2014). The model of multiphase machines involves more electrical parameters and the phase currents are decomposed into more subspaces due to the higher number of degrees of freedom, making more difficult the sensitive analysis with respect to the three-phase case.

The purpose of this paper is therefore the experimental investigation of the parameter detuning impact on the performance of a controlled five-phase induction machine (IM), one of the most interesting multiphase drives (Barrero and Duran, 2016; Levi, 2016). The FCS-MPC method is used to control the stator currents, and an outer PI control loop regulates the machine speed. This speed controller is based on a conventional Indirect Rotor Field Oriented Control (IRFOC) where the usual four inner PI current regulators are replaced by the FCS-MPC current control. Each electrical parameter of the machine will be individually tested for several operating points in order to identify the system variables principally affected by each parameter. The rest of the paper is organized as follows. The model of the five-phase IM drive is presented in Section 2. Then, the general control scheme, which is composed by a FCS-MPC based current controller and an outer speed control, is shown in Section 3. Section 4 presents the principles for the sensitivity analysis and the obtained experimental results are shown in Section 5. Conclusions are summarized in the last section.

2. Modeling of the multiphase system

A five-phase IM with distributed windings equally displaced ($\vartheta = 2\pi/5$) and fed by a five-phase two-level VSI constitutes the system under study. A schematic layout of the drive is presented in Fig. 1, where the VSI gating signals are represented by $(S_a, ..., S_e)$ together with their complementary values $(\bar{S}_a, ..., \bar{S}_e)$. The modeling of the five-phase machine and the VSI are presented in the following subsections.

2.1. Five-phase IM model

During the modeling process, some simplifications are normally made in the machine equations to facilitate the real-time implementation of the control technique. Thus, the following standard assumptions are made: uniform air gap, symmetrical distributed windings, sinusoidal MMF distribution, and negligible core losses and magnetic saturation. Following the Vector Space Decomposition (VSD) approach and taking into account the previous simplifications, the machine model can be represented in state space matrix form in two orthogonal subspaces (Levi et al., 2007) as follows

$$\begin{aligned} \frac{d\boldsymbol{x}(t)}{dt} &= \boldsymbol{A}(\omega_r(t))\,\boldsymbol{x}(t) + \boldsymbol{B}\,\boldsymbol{v}(t) \\ \boldsymbol{y}(t) &= \boldsymbol{C}\,\boldsymbol{x}(t) \end{aligned} \tag{1}$$

where the $\alpha - \beta$ and $x - y$ stator currents and the $\alpha - \beta$ rotor flux are selected as state variables $\boldsymbol{x} = (i_{s\alpha}, i_{s\beta}, i_{sx}, i_{sy}, \psi_{r\alpha}, \psi_{r\beta})^T$, the input signals are the applied stator voltages $\boldsymbol{v} = (v_{s\alpha}, v_{s\beta}, v_{sx}, v_{sy})^T$, and the output signals are the stator currents $\boldsymbol{y} = (i_{s\alpha}, i_{s\beta}, i_{sx}, i_{sy})^T$. The $\alpha - \beta$ subspace corresponds to the fundamental flux and the generated electrical torque, while the $x - y$ subspace is related to the losses. A zero sequence current component in the z-axis also exists, but it does not flow due to the star-winding connection in the machine. In (1) matrices $\boldsymbol{A}$ and $\boldsymbol{B}$ depend on the rotor electric speed ω_r and the electrical machine parameters as it will be shown in the next two equations. The electrical

parameters of the machine are the stator and rotor resistances R_s and R_r, stator and rotor inductances L_s and L_r, stator and rotor leakage inductances L_{ls} and L_{lr} and mutual inductance L_m.

$$\boldsymbol{A} = \begin{pmatrix} a_1 & 0 & 0 & 0 & a_2 & \omega_r a_3 \\ 0 & a_1 & 0 & 0 & -\omega_r a_3 & a_2 \\ 0 & 0 & -\frac{R_s}{L_{ls}} & 0 & 0 & 0 \\ 0 & 0 & 0 & -\frac{R_s}{L_{ls}} & 0 & 0 \\ \frac{L_m R_r}{L_r} & 0 & 0 & 0 & -\frac{R_r}{L_r} & -\omega_r \\ 0 & \frac{L_m R_r}{L_r} & 0 & 0 & \omega_r & -\frac{R_r}{L_r} \end{pmatrix}$$

$$\boldsymbol{B} = \begin{pmatrix} b_1 & 0 & 0 & 0 \\ 0 & b_1 & 0 & 0 \\ 0 & 0 & \frac{1}{L_{ls}} & 0 \\ 0 & 0 & 0 & \frac{1}{L_{ls}} \\ 0 & 0 & 0 & 0 \\ 0 & 0 & 0 & 0 \end{pmatrix} \quad \boldsymbol{C} = \begin{pmatrix} 1 & 0 & 0 & 0 & 0 & 0 \\ 0 & 1 & 0 & 0 & 0 & 0 \\ 0 & 0 & 1 & 0 & 0 & 0 \\ 0 & 0 & 0 & 1 & 0 & 0 \end{pmatrix} \tag{2}$$

$$\begin{aligned} a_1 &= -\frac{R_s L_r^2 + R_r L_m^2}{L_r(L_r L_s - L_m^2)} \\ a_2 &= \frac{R_r L_m}{L_r(L_r L_s - L_m^2)} \\ a_3 &= \frac{L_m}{L_r L_s - L_m^2} \\ b_1 &= \frac{L_r}{L_r L_s - L_m^2} \\ L_s &= L_{ls} + L_m \\ L_r &= L_{lr} + L_m \end{aligned} \tag{3}$$

2.2. Five-phase two-level VSI model

The machine model must be completed with the VSI equations. Each leg of the inverter is composed by two semiconductors operating only in two states, cutoff and saturation (see Fig. 1). Consequently, there exists a finite number of possible combinations of the switching states. For the case of the 5-phase VSI, there are 2^5 possible switching states represented by the vector $\boldsymbol{S_j} = (S_a, S_b, S_c, S_d, S_e)$ with $j = 0, \ldots, 31$.

Ideally, the inverter converts the switching state into phase stator voltages that can be projected into $\alpha-\beta-x-y$ axes following the next equation, where V_{dc} is the DC-link voltage and $\boldsymbol{M}$ is the coordinate transformation matrix that considers the spatial distribution of the machine windings.

$$\begin{pmatrix} v_{s\alpha} \\ v_{s\beta} \\ v_{sx} \\ v_{sy} \end{pmatrix} = \frac{1}{5} V_{dc}\, \boldsymbol{M} \begin{pmatrix} 4 & -1 & -1 & -1 & -1 \\ -1 & 4 & -1 & -1 & -1 \\ -1 & -1 & 4 & -1 & -1 \\ -1 & -1 & -1 & 4 & -1 \\ -1 & -1 & -1 & -1 & 4 \end{pmatrix} \begin{pmatrix} S_a \\ S_b \\ S_c \\ S_d \\ S_e \end{pmatrix} \tag{4}$$

$$\boldsymbol{M} = \frac{2}{5} \begin{pmatrix} 1 & \cos\vartheta & \cos 2\vartheta & \cos 3\vartheta & \cos 4\vartheta \\ 0 & \sin\vartheta & \sin 2\vartheta & \sin 3\vartheta & \sin 4\vartheta \\ 1 & \cos 2\vartheta & \cos 4\vartheta & \cos\vartheta & \cos 3\vartheta \\ 0 & \sin 2\vartheta & \sin 4\vartheta & \sin\vartheta & \sin 3\vartheta \end{pmatrix} \tag{5}$$

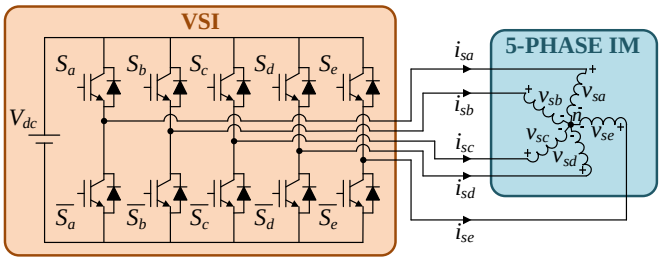

Figure 1: Schematic diagram of the five-phase IM drive.

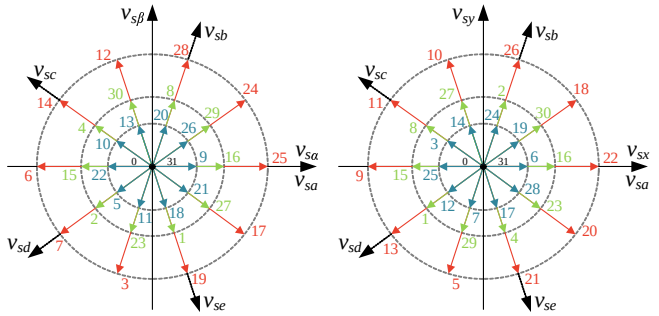

Figure 2: Space vector representation in the $\alpha-\beta$ and $x-y$ subspaces of the possible voltage vectors of the two-level five-phase VSI.

Fig. 2 shows all voltage vectors that can be obtained from the possible switching states. Each vector is identified using the decimal number corresponding to the binary code of the switching state. Equation (4) completes the model of the five-phase IM drive.

3. Speed and current control of the five-phase drive

The general scheme of the proposed control strategy is presented in Fig. 3. It is formed by an IRFOC-based outer speed control loop and an inner FCS-MPC current controller. In following subsections the basis of both controllers are presented.

3.1. IRFOC-based speed controller

Conventional IRFOC technique is composed by an outer speed control loop in the rotating reference frame $d-q$, being the d-axis aligned to the rotor flux component. In this situation, torque and flux production are independently controlled, being the d-current responsible of the rotor flux regulation, while q-current is related to the electrical torque production. In our case, the machine is fluxed by setting a constant value of d-current reference i^*_{sd}, which corresponds with the rated flux of the machine, while i^*_{sq} is obtained from a PI controller. These references in the rotating reference frame are rotated into $\alpha-\beta$ plane using the inverse of the Park transformation

$$\boldsymbol{D^{-1}} = \begin{pmatrix} \cos\theta_e & -\sin\theta_e \\ \sin\theta_e & \cos\theta_e \end{pmatrix} \tag{6}$$

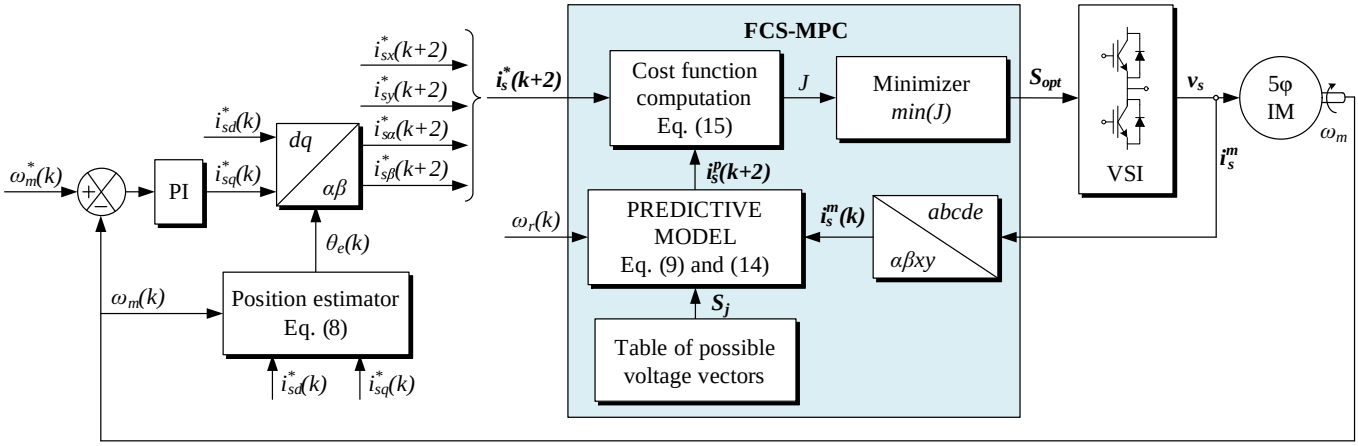

Figure 3: General scheme of the proposed controller composed by an outer IRFOC-based speed loop and an inner FCS-MPC current loop.

being θ_e the angle of the rotating reference frame, which corresponds to the rotor flux angle. This angle is obtained from the measured speed ω_m and the estimated slip speed ω_{sl} in the following way

$$\theta_e = \int (\omega_{sl} + P\,\omega_m)\,dt = \int \left(\frac{R_r}{L_r}\frac{i_{sq}^*}{i_{sd}^*} + P\,\omega_m\right) dt \quad (7)$$

where P is the number of pole pairs. The obtained $\alpha - \beta$ stator current references are inputs in the predictive current control, as it is observed in Fig. 3. In order to be implemented in a microprocessor, equation (7) is discretized using the trapezoidal rule using past values of the variables in the following way

$$\theta_e[k+1] = \theta_e[k] + T_s\,(\omega_{sl}[k] + P\,\omega_m[k]) \quad (8)$$

being T_s the sampling time and considering that the slip and the mechanical speed are constant throughout the prediction horizon.

3.2. FCS-MPC current controller

The applied FCS-MPC current controller is a discrete time algorithm that determines at every sampling time the most adequate switching state $\boldsymbol{S_{opt}}$ that must be applied to track the stator current references $\boldsymbol{i_s^*}$ (see Fig. 3). For this purpose, a discrete model of the real system, named predictive model, is employed to predict the future values of the stator currents $\boldsymbol{i_s^p}$. This prediction is computed for all possible switching states $\boldsymbol{S_j}$ making use of measured values of the rotor speed ω_r and the stator currents $\boldsymbol{i_s^m}$. The most adequate voltage vector is then selected by minimizing a cost function J that relates the current references and predictions. The optimum gating signal is applied to the VSI during the next sampling instant, being this an iterative process repeated every sampling period.

The construction of the prediction model must be done taking into account two important aspects, the discretization method and the delay compensation. The cost function is selected depending on the control objectives.

3.2.1. Discretization process

IM machine equations (1) together with the inverter model (4) define a nonlinear set of equations that represents the real system. These equations must be discretized in order to be implemented in a digital processor. Several discretization alternatives appear, being the first-order forward Euler approximation the most common technique. However, this method is not sufficient under some circumstances, e.g. low sampling frequencies, order of the model higher than one or high pass filters in the plant (Kouro et al., 2015). In those cases, it is better to apply a bilinear discretization or the exact discretization technique, based on the Cayley-Hamilton theorem (Miranda et al. (2009); Rojas et al. (2014)).

In this work, the exact discretization method is applied since it produces better tracking and prediction results in the FCS-MPC performance (Martín et al., 2016b; Miranda et al., 2009). Thus, using a sampling time T_s and assuming that the input is generated by a zero-order hold and matrix $\boldsymbol{A}$ is constant during the sampling period, the discrete predictive model is given by

$$\begin{aligned} \boldsymbol{x^p}[k+1|k] &= \boldsymbol{\Phi}\,\boldsymbol{x^m}[k] + \boldsymbol{\Gamma}\,\boldsymbol{v}[k] \\ \boldsymbol{y^p}[k+1|k] &= \boldsymbol{C}\,\boldsymbol{x^p}[k+1|k] \end{aligned} \quad (9)$$

where $\boldsymbol{\Phi} = e^{\boldsymbol{A}T_s}$ and $\boldsymbol{\Gamma} = \int_0^{T_s} e^{\boldsymbol{A}t}\,\boldsymbol{B}\,dt$. Superscripts $\boldsymbol{p}$ and $\boldsymbol{m}$ represent predicted and measured variables, respectively, being $\boldsymbol{x^p}[k+1|k]$ the one-step ahead prediction of the system state computed at current sample time k. Notice that matrix $\boldsymbol{A}$ depends on the instantaneous value of the rotor electric speed ω_r, thus the above predictive model is a time-variant linear system. However, the dynamics of the mechanical system is slower than the electrical one, so the speed within a sampling period can be assumed constant. Consequently, it is necessary to update the instantaneous value of the matrices $\boldsymbol{\Phi}$ and $\boldsymbol{\Gamma}$ every sampling interval with the measured value of the rotor speed.

In order to simplify the implementation of the equations, some off-line calculations can be done. Firstly, matrix $\boldsymbol{A}$

is separated in a constant part and a speed dependent (or time dependent) part, as follows

$$\boldsymbol{\Phi} = e^{\boldsymbol{A}T_s} = e^{(\boldsymbol{A}_c+\boldsymbol{A}_{\boldsymbol{\omega}})T_s} = e^{\boldsymbol{A}_c T_s}\, e^{\boldsymbol{A}_{\boldsymbol{\omega}} T_s} \tag{10}$$

Since all components of matrix $e^{\boldsymbol{A}_c T_s}$ are constant, it can be obtained off-line. However, matrix $e^{\boldsymbol{A}_{\boldsymbol{\omega}} T_s}$ must be evaluated every sampling period. A simple definition of this matrix can be obtained using the Cayley-Hamilton theorem, as it is shown in the following equation, where $c_\omega = \cos(\omega_r T_s)$ and $s_\omega = \sin(\omega_r T_s)$.

$$e^{\boldsymbol{A}_{\boldsymbol{\omega}} T_s} = \begin{pmatrix} 1 & 0 & 0 & 0 & a_3(1-c_\omega) & a_3 s_\omega \\ 0 & 1 & 0 & 0 & -a_3 s_\omega & a_3(1-c_\omega) \\ 0 & 0 & 1 & 0 & 0 & 0 \\ 0 & 0 & 0 & 1 & 0 & 0 \\ 0 & 0 & 0 & 0 & c_\omega & -s_\omega \\ 0 & 0 & 0 & 0 & s_\omega & c_\omega \end{pmatrix} \tag{11}$$

Regarding matrix $\boldsymbol{\Gamma}$, it can be approximated using the expression in (12) assuming that the time-dependent terms are canceled ($e^{\boldsymbol{A}_{\boldsymbol{\omega}} T_s}\boldsymbol{B} = \boldsymbol{B}$) when a small enough sampling time T_s is used (Rojas et al., 2014). However, a simpler approximation of this matrix can be done using the right Riemann sum method in a time interval equal to a sampling period, and assuming again that the sampling time is small enough (13). Notice that the dependence with the rotor speed disappear, being possible to obtain matrix $\boldsymbol{\Gamma}$ by off-line calculations.

$$\boldsymbol{\Gamma} = \int_0^{T_s} e^{\boldsymbol{A}_c t}\, \boldsymbol{B}\, dt = A_c^{-1}(e^{\boldsymbol{A}_c T_s} - \boldsymbol{I})\boldsymbol{B} \tag{12}$$

$$\boldsymbol{\Gamma} = \int_0^{T_s} e^{\boldsymbol{A}_c t}\, \boldsymbol{B}\, dt = e^{\boldsymbol{A}_c T_s}\, \boldsymbol{B} T_s \tag{13}$$

Both approximations, (12) and (13), can be applied without loss of generality since they produce similar results when the sampling time is small. In this case, the second one is applied in order to simplify the calculations.

3.2.2. Delay compensation

In any digitally implemented controller, such as FCS-MPC, the calculation time of the control signal can be significant compared with the sampling time. In this case, there will be an important delay between the instant when system variables (stator currents) are measured and used for prediction, and the instant when the next control action is released. As a result, the optimal control action is not applied in the correct instant producing a bad tracking of the currents, which can present a high ripple. This effect and its consequences are properly explained in Cortes et al. (2012) for a three-phase converter controlled by the FCS-MPC. In order to correct this effect, some compensation methods have been proposed in the literature. The most simple one consists in waiting until the next sampling time to release the computed switching state based on a prediction model for the instant $k+2$ (Cortes et al. (2012); Arahal et al. (2009)). Taking this into account, the control algorithm is changed to reflect that the control action computed at time k will not affect the system output until time $k+2$. This is achieved applying two prediction steps: a first one uses (9) to compute the current prediction for $k+1$, and a second one computes the second-step ahead prediction as

$$\boldsymbol{x}^{\boldsymbol{p}}[k+2|k] = \boldsymbol{\Phi}\, \boldsymbol{x}^{\boldsymbol{p}}[k+1|k] + \boldsymbol{\Gamma}\, \boldsymbol{v}[k+1] \tag{14}$$

The optimization process of the cost function will be then implemented taking into account the current prediction in $k+2$ for all possible voltage vectors $\boldsymbol{v}[k+1]$.

3.2.3. Cost function

As stated before, the cost function must be defined according to the control objective, which consists in tracking the stator current references. In the case of multiphase IM drives, the following expression is usually employed

$$J = \|\boldsymbol{i}^*_{\boldsymbol{s\alpha\beta}}[k+2] - \boldsymbol{i}^{\boldsymbol{p}}_{\boldsymbol{s\alpha\beta}}[k+2|k]\|^2 + \lambda_{xy}\|\boldsymbol{i}^{\boldsymbol{p}}_{\boldsymbol{sxy}}[k+2|k]\|^2 \tag{15}$$

where $\boldsymbol{i_{s\alpha\beta}} = (i_{s\alpha}, i_{s\beta})$, $\boldsymbol{i_{sxy}} = (i_{sx}, i_{sy})$ and $\alpha-\beta$ references are the ones obtained as outputs of the PI controller. The error between the predicted stator currents and their references is then minimized, and the weighting factor λ_{xy} is introduced to give more or less importance to the secondary $x-y$ plane with respect to the primary $\alpha-\beta$ plane. This parameter must be properly adjusted in order to favor a good flux/torque production but with reasonably small current ripple in the $x-y$ currents.

The selection of the weighting factor is also closely related to the number of possible switching states employed in the optimization process. In Lim et al. (2014) a good analysis on this issue is realized, concluding that the reduction in the available voltage vectors interferes in the selection of λ_{xy}, since the control performance can change significantly. In this work, the weighting factor is set to 0.5, since it has been proved to produce a good trade-off between current ripple in the primary plane and the secondary one when all possible VSI switching states are available (Lim et al., 2014). Additional terms can be included in the cost function in order to improve other features such as reducing the VSI losses or the Total Harmonic Distortion (THD) (Kouro et al., 2009).

4. Basis of the sensitivity analysis

An experimental testbench has been constructed to study the impact of the electrical parameters in the development of the proposed controller. The components of the testbench are depicted in Fig. 4. The principal element is a five-phase IM, whose parameters have been experimentally obtained following the method described in Yepes et al. (2012) and Riveros et al. (2012) and are summarized in Table 1. Two three-phase inverters from Semikron fed the five-phase machine using an independent DC power supply of 300 V as DC-link voltage. The control algorithm is

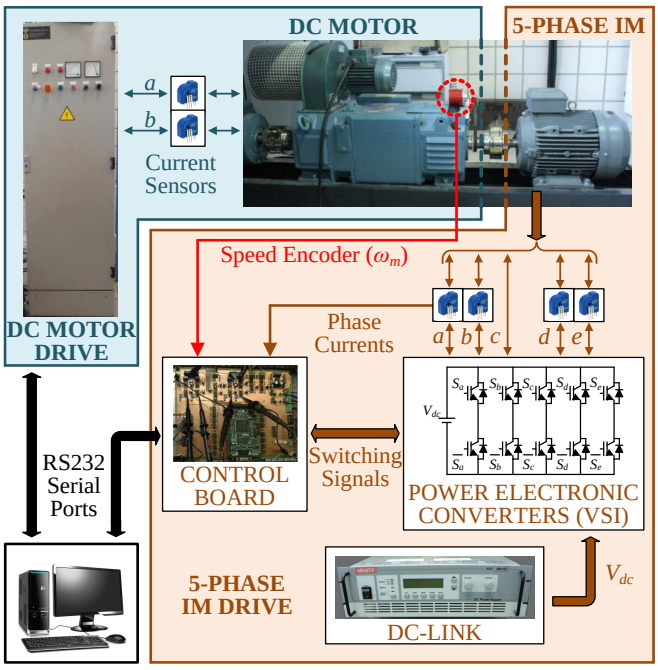

Figure 4: Experimental testbench diagram. The real system is based on two conventional three-phase VSIs, an electronic control board, a DC motor drive, an IM and a DC motor.

Table 1: Parameters of the analyzed five-phase IM.

Parameter		Value
Stator resistance	$R_{s0}(\Omega)$	19.45
Rotor resistance	$R_{r0}(\Omega)$	6.77
Stator leakage inductance	L_{ls0}(mH)	100.7
Rotor leakage inductance	L_{lr0}(mH)	38.6
Mutual inductance	L_{m0}(mH)	656.5
Mechanical nominal speed	ω_n(rpm)	1000
Nominal torque	T_n(N·m)	4.7
Pole pairs	p	3

deployed in a TM320F28335 DSP placed on a MSK28335 Technosoft board. The measurement of the mechanical rotor speed is carried out by a GHM510296R/2500 digital encoder together with the enhanced quadrature encoder pulse (eQEP) peripheral of the DSP. Finally, a DC motor directly coupled to the shaft of the multiphase IM introduces a variable load torque in the system.

The IRFOC-based speed and the FCS-MPC current controllers have been implemented as stated in Section 3 using all possible voltage vectors and $\lambda_{xy} = 0.5$ in the optimization process, a sampling time of $T_s = 66.67$ μs and a constant d-current reference of 0.57 A, which corresponds with the rated flux of the five-phase IM. To reproduce the parameter detuning, parameters in the predictive model (14) in relation with the stator (R_s and L_{ls}) and the magnetic coupling (L_m) are varied one at a time in order to investigate the individual effect of each parameter in the performance of the system. The rotor parameters (R_r and L_{lr}) are simultaneously varied, thus representing the effect of the rotor branch in the control performance. In what follows, the nominal parameters will be called R_{s0}, R_{r0}, L_{ls0}, L_{lr0} and L_{m0} (see Table 1), and the parameter variations will be represented by $\Delta R_s = R_s/R_{s0}$, $\Delta R_r = R_r/R_{r0}$, $\Delta L_{ls} = L_{ls}/L_{ls0}$, $\Delta L_{lr} = L_{lr}/L_{lr0}$ and $\Delta L_m = L_m/L_{m0}$.

Three different tests have been conducted varying the operating condition of the multiphase drive, i.e. mechanical speed ω_m and the load torque T_L, in order to study the effect of these variables in the sensitivity analysis. Table 2 summarizes the operating conditions of each test, being the load torque expressed as the percentage of the nominal one (T_n in Table 1). Two different values of the speed and the load have been selected with enough distance between them in order to produce significant comparison results. Steady state operation is always achieved for all tests. Root-Mean-Squared (RMS) error between the reference and the measured phase stator currents ($RMSe_p$), and mean (μ) and standard deviation (σ) of the system variables are used as performance indicators

$$RMSe_p = \frac{1}{5}\sum_{m=a}^{e}\sqrt{\frac{1}{N}\sum_{j=1}^{N}(i_{sm}(j) - i^*_{sm}(j))^2} \tag{16}$$

$$\mu = \frac{1}{N}\sum_{j=1}^{N} var(j) \tag{17}$$

$$\sigma = \sqrt{\frac{1}{N}\sum_{j=1}^{N}(var(j) - \mu)^2} \tag{18}$$

where var represents the system variable whose mean and deviation values are evaluated. Between 50 and 60 trials have been reproduced for studying the R_s, L_{ls} and L_m mismatch, while around 90 trials were obtained to study the variation of the rotor parameters.

5. Obtained results

The control performance in terms of the $RMSe_p$ for the three considered operating points is shown in Fig. 5 when mutual inductance L_m, stator leakage inductance L_{ls} and stator resistance R_s are varied. From the obtained results it can be stated that L_m has a significant impact in the phase current RMS error when the parameter is incremented, although no impact in the $RMSe_p$ value is obtained when the used L_m value is lower than the nominal one (L_{m0}), see Fig. 5a. Moreover, when the operating point is varied and the machine speed and load torque are increased, the effect of L_m in the control performance also increases. Thus, the current error rapidly raises above $\Delta L_m = 1.4$ in Test 2 and $\Delta L_m = 1$ in Test 3. On the contrary, current error begins to grow only after $\Delta L_m = 1.8$ in Test 1 and a very high detuning in the mutual inductance must be introduced to see a significant impact in the current tracking for lower speed and torque operating conditions.

Fig. 5b shows the impact of L_{ls} variations, where a ΔL_{ls} value from 0.2 to 4 has been considered. It is observed that

Table 2: Experimental conditions of the study.

Test	ω_m (rpm)	T_L (%)
1	600	40
2	600	60
3	800	40

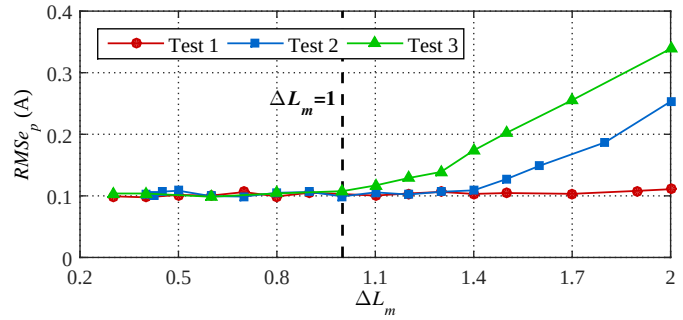

(a)

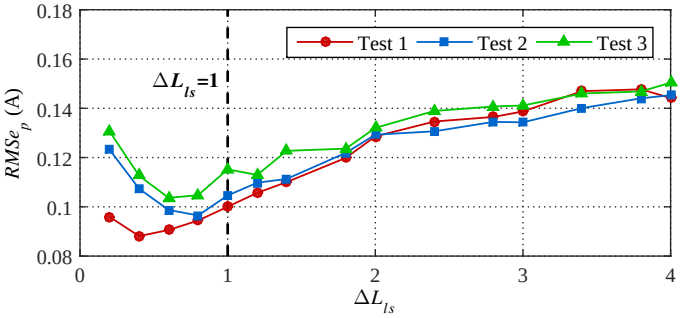

(b)

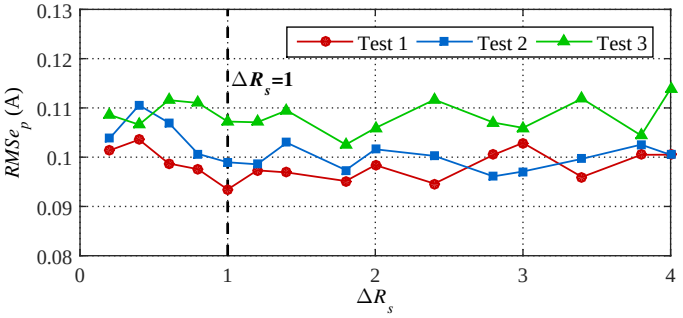

(c)

Figure 5: Obtained $RMSe_p$ values for Tests 1, 2 and 3 when (a) L_m, (b) L_{ls} and (c) R_s are varied.

current tracking performance gradually degenerates when ΔL_{ls} increases. On the contrary, when the L_{ls} value is inferior to the nominal one ($\Delta L_{ls} < 1$), the obtained $RMSe_p$ value decreases until a minimum value appears (this minimum depends on the operating condition, but it is always close to $\Delta L_{ls} = 0.5$) to abruptly rise for lower L_{ls} values. Notice however that the total variation of the $RMSe_p$ value is about 0.06 A in the considered ΔL_{ls} range, concluding that the impact of the stator leakage inductance in the system performance is not relevant in comparison with other parameters. As in the previous case, the current error is higher for larger speed and load torque values if $\Delta L_{ls} < 1$, but the tracking performance does not show significant differences when ΔL_{ls} increases.

Regarding the stator resistance, its influence is analyzed in Fig. 5c. The ΔR_s ratio is varied from 0.2 to 4 for the studied operating points. It is shown that the current control performance almost stays unaltered when the parameter is varied, being $RMSe_p$ larger when the load torque and the rotor speed increase, as in previous cases.

The effect of the rotor electrical parameters in the current control performance is analyzed in Fig. 6. In this case, R_r and L_{lr} are simultaneously varied from 0.2 to 2 times their nominal values. Surface plots represent the $RMSe_p$ error in the considered operating points. It can be concluded from the obtained results that L_{lr} has not a significant impact in the current control performance (the curves mainly remain the same independently of the ΔL_{lr} value). On the contrary, the variation of the R_r parameter has an important effect in the current tracking error, particularly if $R_r < R_{r0}$, and larger speed and load torque values increase the obtained $RMSe_p$ value.

To provide a better insight of this sensitivity analysis, the mean (μ) and standard deviation (σ) of system variables have been calculated using (17) and (18). The mean value is used as an indicator of the tracking performance while the standard deviation is related to the noise of the electrical system. The analyzed variables are the mechanical speed (ω_m), $d-q$ currents (i_d and i_q), q-current reference (i_q^*) and $x-y$ currents (i_x and i_y). Figs. 7 to 10 present the obtained results where μ is depicted as a solid line with square or circle markers and σ is represented as solid vertical lines around the markers. Notice that only one operating point is shown for simplicity reasons (similar plots are obtained for different operating points).

Results when parameter L_m is varied are presented in Fig. 7. It can be noticed that the current control is degraded when ΔL_m increases, which agrees with Fig. 5a. The electrical noise remains the same in the primary $d-q$ plane. However, an important deviation of μ values appears, particularly in the q-axis. Currents in the secondary $x-y$ plane fit their references, but σ increases with ΔL_m, as well as the electrical noise in the $x-y$ components and the harmonic content and copper losses of the system. It is important to note that a mismatch in the L_m parameter of the predictive model also affects the position estimator of the IRFOC-based speed loop (7), which disarranges the outer speed control loop. This effect can be appreciated in the speed controller output (i_q^* value) that increases when L_m differs from L_{m0}. Despite this, the speed tracking is good and it is not affected in the studied ΔL_m range.

Fig. 8 summarizes the obtained results when a variation in the R_r parameter is considered. In this particular case, the speed regulation offers a similar response than in the previous case, when L_m is varied, but the current performance in the $d-q$ and $x-y$ planes is the opposite. The current control performance when ΔR_r is increased is then

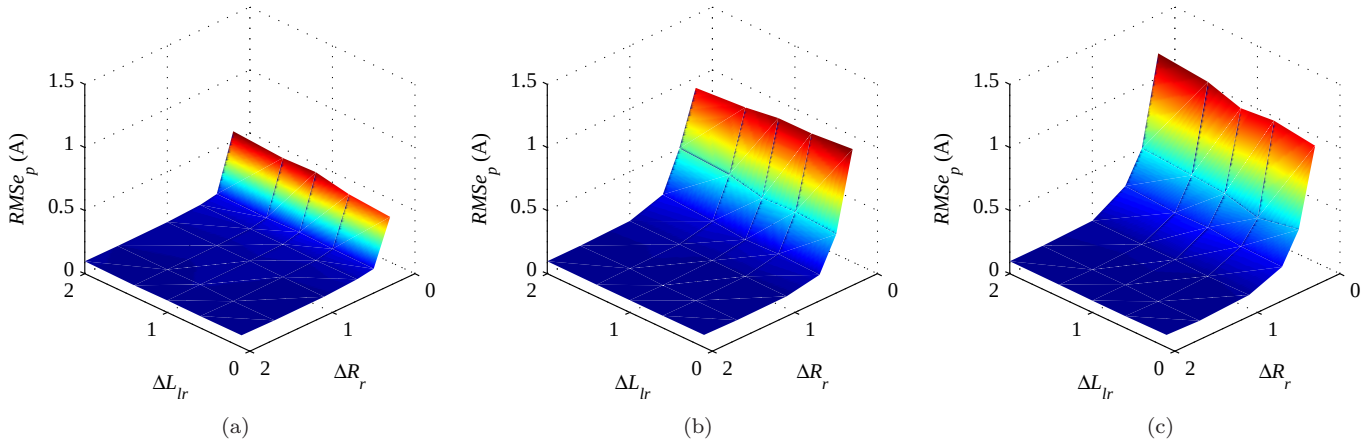

Figure 6: Obtained $RMSe_p$ values for simultaneous R_r and L_{lr} variation for (a) Test 1, (b) Test 2 and (c) Test 3.

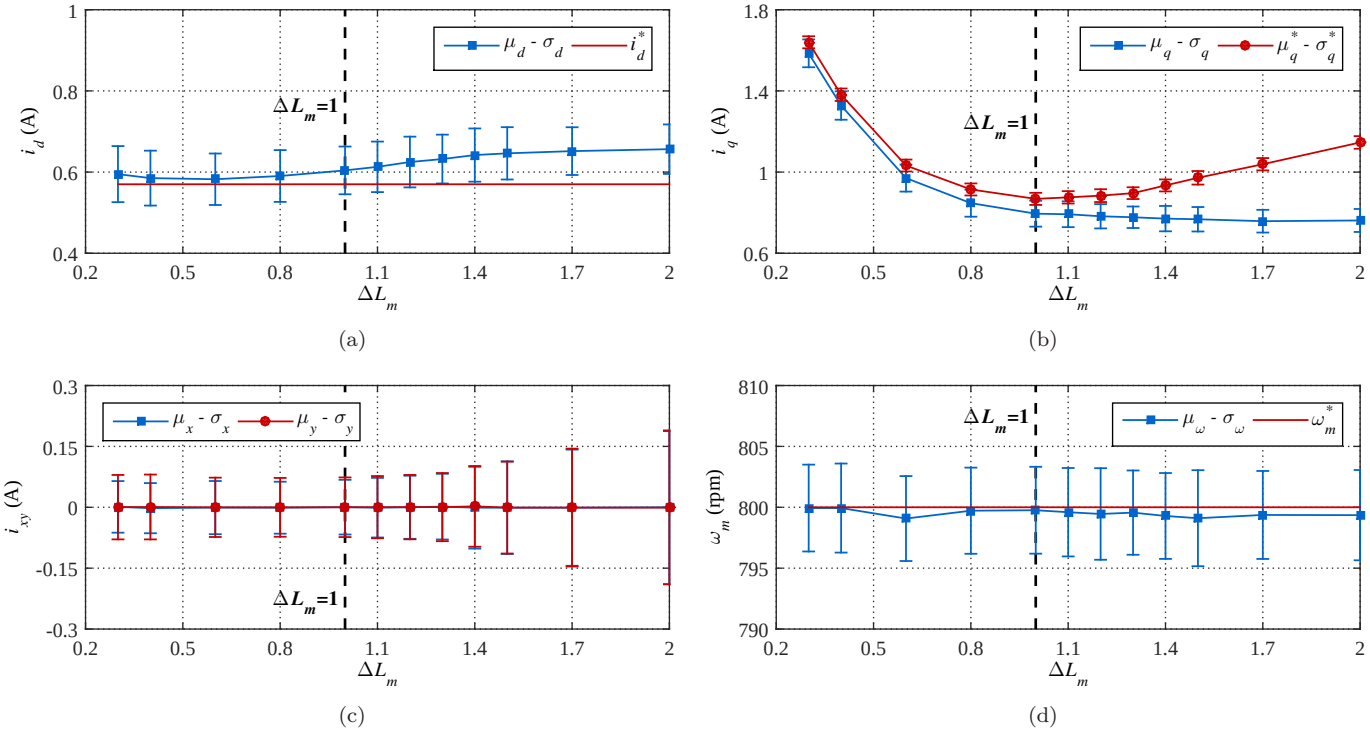

Figure 7: Control performance when the applied L_m differs from the nominal one (L_{m0}). (a) Mean and standard deviation of the measured stator d-current (μ_d, σ_d) and the imposed stator d-current reference (i_d^*), (b) mean and standard deviation of the measured stator q-current (μ_q, σ_q) and the generated stator q-current reference (μ_q^*, σ_q^*), (c) mean and standard deviation of x- and y- currents (μ_x, σ_x, μ_y, σ_y), and (d) mean and standard deviation of ω_m (μ_ω, σ_ω) and its reference (ω_m^*).

similar to the situation when ΔL_m is decreased and vice versa, being this result in agreement with those obtained in Fig. 6 and Fig. 5a.

The effect of the L_{ls} variation is depicted in Fig. 9. As in previous cases, the speed regulation is not altered by the parameter mismatch, but the current control performance is distorted. While the d-current mean (μ_d) remains close to its reference when ΔL_{ls} is higher than one, the standard deviation (σ_d) increases as a consequence of larger electrical noises. The opposite behavior is observed when ΔL_{ls} is lower than one, but μ_d and i_d^* values pull apart. On the other hand, the q-current tracking performance and the $x-y$ current noise are slightly degraded when ΔL_{ls} increases and decreases from $\Delta L_{ls}=0.5$ (this value corresponds to the minimum $RMSe_p$ value in Fig. 5b). Notice however that the variation in the current performance due to the L_{ls} uncertainty is minimum in comparison with other parameters and can be neglected. Note also

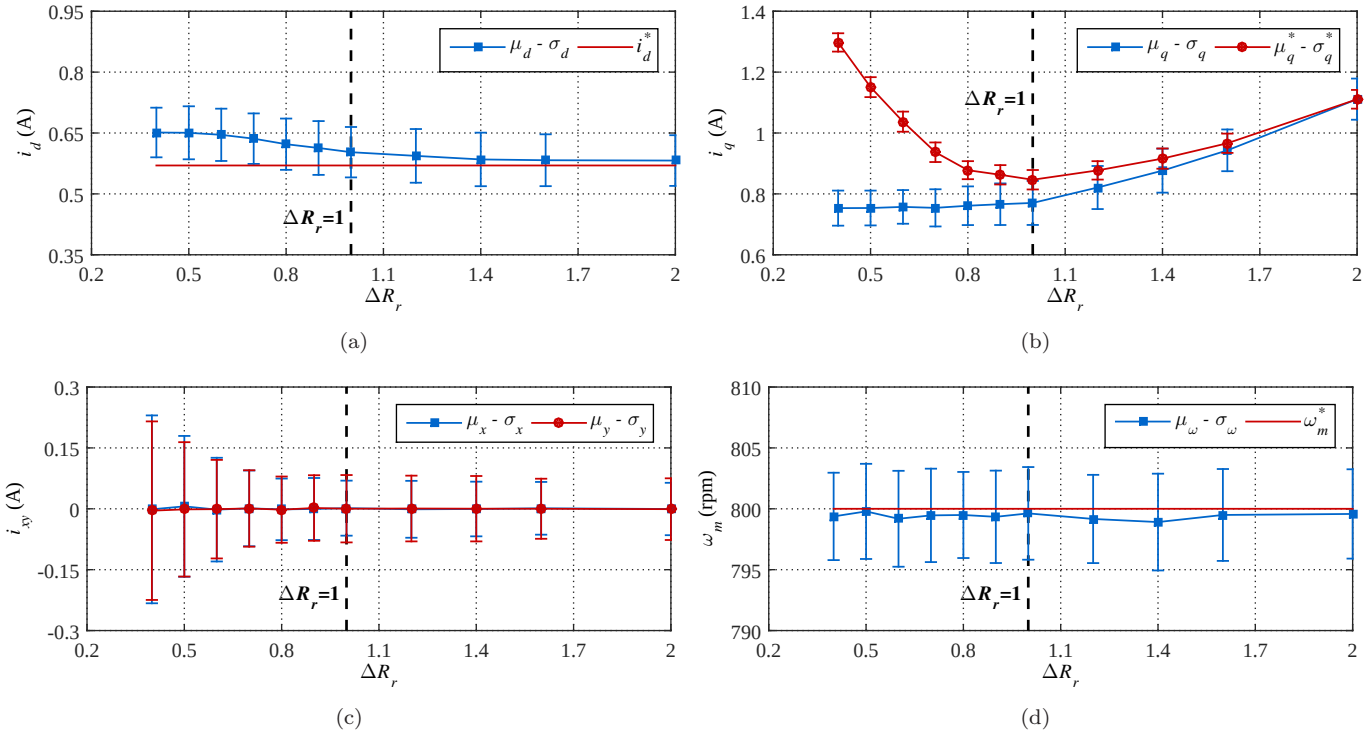

Figure 8: Control performance when the applied R_r differs from the nominal one (R_{r0}). (a) Mean and standard deviation of the measured stator d-current (μ_d, σ_d) and the imposed stator d-current reference (i_d^*), (b) mean and standard deviation of the measured stator q-current (μ_q, σ_q) and the generated stator q-current reference (μ_q^*, σ_q^*), (c) mean and standard deviation of x- and y- currents (μ_x, σ_x, μ_y, σ_y), and (d) mean and standard deviation of ω_m (μ_ω, σ_ω) and its reference (ω_m^*).

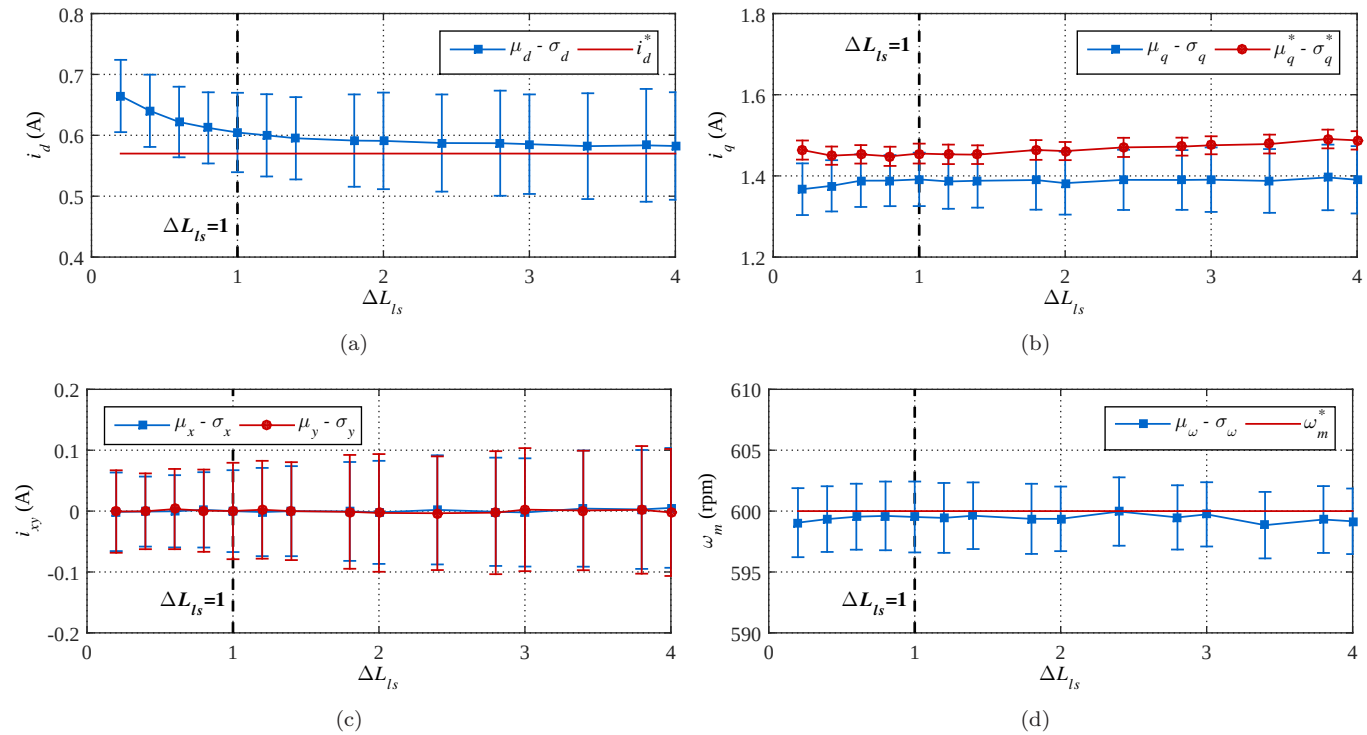

Figure 9: Control performance when the applied L_{ls} differs from the nominal one (L_{ls0}). (a) Mean and standard deviation of the measured stator d-current (μ_d, σ_d) and the imposed stator d-current reference (i_d^*), (b) mean and standard deviation of the measured stator q-current (μ_q, σ_q) and the generated stator q-current reference (μ_q^*, σ_q^*), (c) mean and standard deviation of x- and y- currents (μ_x, σ_x, μ_y, σ_y), and (d) mean and standard deviation of ω_m (μ_ω, σ_ω) and its reference (ω_m^*).

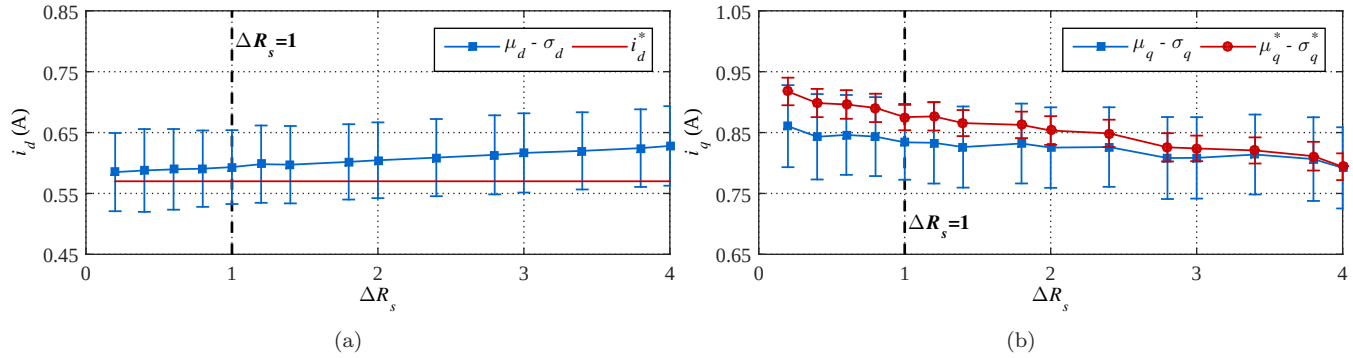

Figure 10: Control performance when the applied R_s differs from the nominal one (R_{s0}). (a) Mean and standard deviation of the measured stator d-current (μ_d, σ_d) and the imposed stator d-current reference (i_d^*), and (b) mean and standard deviation of the measured stator q-current (μ_q, σ_q) and the generated stator q-current reference (μ_q^*, σ_q^*).

Table 3: Qualitative obtained results of the sensitivity analysis.

Impact on the system performance	ΔL_m		ΔR_r		ΔL_{ls}	ΔR_s	ΔL_{lr}
	$\in [0.3, 1]$	$\in [1, 2]$	$\in [0.2, 1]$	$\in [1, 2]$	$\in [0.2, 4]$	$\in [0.2, 4]$	$\in [0.2, 2]$
Speed performance	–	–	–	–	–	–	–
Phase current RMS error	–	↑↑↑	↑↑↑	–	↑	–	–
d current performance	–	↑↑	↑↑	–	↑↑	↑	–
q current performance	–	↑↑↑	↑↑↑	–	↑	↑	–
$x-y$ current performance	–	↑↑↑	↑↑↑	–	↑	–	–

that a steady state error in the $d-q$ current components exists even when there is no mismatch in the model parameters, which is an inherent feature of predictive control techniques that does not have an integral term to overcome this error (Young et al., 2016).

The system performance under R_s variations is finally detailed in Fig. 10. In this case, only the mean and the deviation of the $d-q$ currents are shown since the $x-y$ currents and speed performances are not affected by the mismatch. Obtained results show that σ values in the $d-q$ plane are almost constant for all ΔR_s values. However, the current tracking is degraded in the d- and q-axis when ΔR_s increases and decreases, respectively. These contradictory effects counteract resulting in almost constant current tracking performance, as it was shown in Fig. 5c. Additionally, taking into account that a normal variation of the stator resistance can be $\pm 50\%$ of the nominal value due to thermal effects, its impact in the torque and flux tracking can be considered not significant.

These results are summarized in Table 3 (the $-$ symbol means that the impact of the parameter is negligible), where a qualitative analysis of the parameter mismatch effect on different control aspects is presented. It can be concluded that:

- The speed control performance is unaltered by the parameter mismatch.
- The performance of the FCS-MPC controller in terms of phase current tracking is degraded by the parameter mismatch, being different the impact of each machine parameter and having the operating point a notable influence in the sensitivity analysis due to its dependency on the electrical parameters of the machine. While L_m and R_r are highly influential, L_{ls} hardly affects the current tracking and the impact of R_s and L_{lr} is nearly negligible.
- The q-current tracking performance and the electrical noise in the $x-y$ plane are notably affected by L_m and R_r mismatching.
- The current tracking performance in the d-axis is little distorted by a variance in the L_{ls} parameter, which also produces some electrical noise in the $x-y$ plane and almost negligible q-current tracking distortion.

6. Conclusion

In this work, the impact of model parameter mismatch on the performance of the FCS-MPC has been experimentally assessed in five-phase IM drives. Obtained results show that the best estimate of the mutual inductance and the rotor resistance produces the lowest current control degradation, current tracking error and electrical noise in the $x-y$ current components, which improves the torque and flux control in the electrical drive and reduces the harmonic content and copper losses in the system. Conversely,

the influence of stator resistance and leakage inductances in the close loop current control performance are not so important, as long as the parameters are within a normal range of variation. However, the speed regulation is robust against parameter mismatch due to the outer PI regulator. The experimental results also show that the operating point can promote the parameter mismatch effects, and higher steady-state errors are observed for higher motor speeds and load torques.

Acknowledgments

The authors would like to thank the University of Seville and the Ministerio de Economía y Competitividad of the Spanish Government for their funding under VPPI-US, DPI2013-44278-R and ENE2014-52536-C2-1-R programs.

References

Arahal, M. R., Barrero, F., Toral, S., Duran, M. J., Gregor, R., 2009. Multi-phase current control using finite-state model-predictive control. Control Engineering Practice 17 (5), 579–587.

Barrero, F., Duran, M. J., Jan 2016. Recent advances in the design, modeling, and control of multiphase machines - partI. IEEE Transactions on Industrial Electronics 63 (1), 449–458.

Chai, S., Wang, L., Rogers, E., 2013. Model predictive control of a permanent magnet synchronous motor with experimental validation. Control Engineering Practice 21 (11), 1584–1593.

Cortes, P., Rodriguez, J., Silva, C., Flores, A., 2012. Delay compensation in model predictive current control of a three-phase inverter. IEEE Transactions on Industrial Electronics 59 (2), 1323–1325.

Jung, E., Yoo, H., Sul, S. K., Choi, H. S., Choi, Y. Y., May 2012. A nine-phase permanent-magnet motor drive system for an ultrahigh-speed elevator. IEEE Transactions on Industry Applications 48 (3), 987–995.

Kouro, S., Cortes, P., Vargas, R., Ammann, U., Rodriguez, J., June 2009. Model predictive control - a simple and powerful method to control power converters. IEEE Transactions on Industrial Electronics 56 (6), 1826–1838.

Kouro, S., Perez, M. A., Rodriguez, J., Llor, A. M., Young, H. A., 2015. Model predictive control: Mpc's role in the evolution of power electronics. IEEE Industrial Electronics Magazine 9 (4), 8–21.

Kwak, S., Moon, U. C., Park, J. C., Nov 2014. Predictive-control-based direct power control with an adaptive parameter identification technique for improved AFE performance. IEEE Transactions on Power Electronics 29 (11), 6178–6187.

Levi, E., 2016. Advances in converter control and innovative exploitation of additional degrees of freedom for multiphase machines. IEEE Transactions on Industrial Electronics 63 (1), 433–448.

Levi, E., Barrero, F., Duran, M. J., Jan 2016. Multiphase machines and drives - revisited. IEEE Transactions on Industrial Electronics 63 (1), 429–432.

Levi, E., Bojoi, R., Profumo, F., Toliyat, H. A., Williamson, S., 2007. Multiphase induction motor drives - a technology status review. IET Electric Power Applications 1 (4), 489–516.

Lim, C. S., Levi, E., Jones, M., Rahim, N. A., Hew, W. P., 2014. FCS-MPC-based current control of a five-phase induction motor and its comparison with PI-PWM control. IEEE Transactions on Industrial Electronics 61 (1), 149–163.

Lim, C. S., Rahim, N. A., Hew, W. P., Levi, E., Jan 2013. Model predictive control of a two-motor drive with five-leg-inverter supply. IEEE Transactions on Industrial Electronics 60 (1), 54–65.

Liu, J., Huang, L., Yu, H., Wen, C., Zhong, W., June 2014. Study on the characteristics of a novel six-phase fault-torrent linear permanent magnet machine for linear oil pumping. IEEE Transactions on Applied Superconductivity 24 (3), 1–5.

Martín, C., Arahal, M. R., Barrero, F., Durán, M. J., 2016a. Multiphase rotor observers for current predictive control: a five-phase case study. Control Engineering Practice 49, 101–111.

Martín, C., Arahal, M. R., Barrero, F., Durn, M. J., 2016b. Five-phase induction motor rotor current observer for finite control set model predictive control of stator current. IEEE Transactions on Industrial Electronics 63 (7), 4527–4538.

Miranda, H., Cortes, P., Yuz, J. I., Rodriguez, J., June 2009. Predictive torque control of induction machines based on state-space models. IEEE Transactions on Industrial Electronics 56 (6), 1916–1924.

Morel, F., Lin-Shi, X., Retif, J. M., Allard, B., Buttay, C., July 2009. A comparative study of predictive current control schemes for a permanent-magnet synchronous machine drive. IEEE Transactions on Industrial Electronics 56 (7), 2715–2728.

Riveros, J. A., Barrero, F., Levi, E., Durán, M. J., Toral, S., Jones, M., 2013. Variable-speed five-phase induction motor drive based on predictive torque control. IEEE Transactions on Industrial Electronics 60 (8), 2957–2968.

Riveros, J. A., Yepes, A., Barrero, F., Doval-Gandoy, J., Bogado, B., Lopez, O., Jones, M., Levi, E., 2012. Parameter identification of multiphase induction machines with distributed windings - part 2: Time-domain techniques. IEEE Transactions on Energy Conversion 27 (4), 1067–1077.

Rodriguez, J., Kazmierkowski, M. P., Espinoza, J. R., Zanchetta, P., Abu-Rub, H., Young, H. A., Rojas, C. A., May 2013. State of the art of finite control set model predictive control in power electronics. IEEE Transactions on Industrial Informatics 9 (2), 1003–1016.

Rojas, C. A., Yuz, J. I., Silva, C. A., Rodriguez, J., 2014. Comments on "Predictive torque control of induction machines based on state-space models". IEEE Transactions on Industrial Electronics 61 (3), 1635–1638.

Siami, M., Khaburi, D. A., Abbaszadeh, A., Rodrguez, J., June 2016. Robustness improvement of predictive current control using prediction error correction for permanent-magnet synchronous machines. IEEE Transactions on Industrial Electronics 63 (6), 3458–3466.

Vatani, M., Bahrani, B., Saeedifard, M., Hovd, M., May 2015. Indirect finite control set model predictive control of modular multilevel converters. IEEE Transactions on Smart Grid 6 (3), 1520–1529.

Wang, F., Zhang, Z., Davari, A., Rodríguez, J., Kennel, R., 2014. An experimental assessment of finite-state predictive torque control for electrical drives by considering different online-optimization methods. Control Engineering Practice 31, 1–8.

Yepes, A. G., Riveros, J. A., Doval-Gandoy, J., Barrero, F., Lopez, O., Bogado, B., Jones, M., Levi, E., 2012. Parameter identification of multiphase induction machines with distributed windings - part 1: Sinusoidal excitation methods. IEEE Transactions on Energy Conversion 27 (4), 1056–1066.

Young, H. A., Perez, M. A., Rodriguez, J., May 2016. Analysis of finite-control-set model predictive current control with model parameter mismatch in a three-phase inverter. IEEE Transactions on Industrial Electronics 63 (5), 3100–3107.

Young, H. A., Perez, M. A., Rodriguez, J., Abu-Rub, H., 2014. Assessing finite-control-set model predictive control: A comparison with a linear current controller in two-level voltage source inverters. IEEE Industrial Electronics Magazine 8 (1), 44–52.

Zhang, X., Hou, B., Mei, Y., 2016. Deadbeat predictive current control of permanent magnet synchronous motors with stator current and disturbance observer. IEEE Transactions on Power Electronics PP (99), 1–1.